BMC Medical Imaging

RESEARCH Open Access

Machine learning prediction model for functional prognosis of acute ischemic stroke based on MRI radiomics of white matter hyperintensities

Yayuan Xia[1], Linhui Li[2], Peipei Liu[3], Tianxu Zhai[4] and Yibing Shi[1,3*]

Abstract

Objective The purpose of the current study is to explore the value of a nomogram that integrates clinical factors and MRI white matter hyperintensities (WMH) radiomics features in predicting the prognosis at 90 days for patients with acute ischemic stroke (AIS).

Methods A total of 202 inpatients with acute anterior circulation ischemic stroke from the Department of Neurology, Xuzhou Central Hospital between September 2023 and March 2024 were retrospectively enrolled. Inpatient clinical data and cranial MRI images were acquired. In this study, the sample was randomly divided into a training cohort comprising 141 cases and a validation cohort of 61 cases in a 7:3 ratio. WMH lesions on fluid-attenuated inversion recovery (FLAIR) sequences were automatically segmented and manually adjusted using Matlab and ITK-SNAP software. The segmentation led to the identification of total white matter hyperintensity (TWMH), periventricular white matter hyperintensity (PWMH), and deep white matter hyperintensity (DWMH). Subsequently, radiomics features were meticulously extracted from these three distinct regions of interest (ROIs). Radiomic models for the three ROIs were developed using six machine learning algorithms. The clinical model was built by identifying clinical risk factors through univariate and multivariate logistic regression analyses. A combined model was subsequently developed incorporating the best radiomics model with significant clinical factors. To illustrate these risk factors, a graphical representation known as a nomogram was devised.

Results Age, previous stroke history, coronary artery disease, admission blood glucose levels, homocysteine levels, and infarct volume were identified as independent clinical predictors of AIS prognosis. A total of 16, 21, and 22 radiomics features were selected from TWMH, PWMH, and DWMH, respectively. The TWMH radiomics model using the SVM classifier exhibited the best predictive performance for AIS prognosis, achieving a sensitivity of 90.0%, a specificity of 81.3%, an accuracy of 85.3%, and an AUC of 0.916 in the validation set. The combined model outperformed both the clinical and radiomics models, exhibiting exceptional predictive capabilities with a validation cohort sensitivity of 89.3%, specificity of 84.8%, accuracy of 86.9%, and AUC of 0.939.

*Correspondence:
Yibing Shi
ctsyb70496@163.com

Full list of author information is available at the end of the article

Conclusion The FLAIR sequence-based WMH radiomics approach demonstrates effective prediction of the 90-day functional prognosis in patients with AIS. The integration of TWMH radiomics and clinical factors in a combined model exhibits superior performance. This innovative model shows potential in aiding clinicians to enhance their assessment of patient prognosis and tailor personalized treatment strategies.

Clinical trial number Not applicable.

Keywords White matter hyperintensities, Acute ischemic stroke, Magnetic resonance imaging, Radiomics, Machine learning

Introduction

In individuals afflicted with acute ischemic stroke (AIS), cranial MRI scans frequently reveal a significant prevalence of white matter hyperintensities (WMH) [1]. WMH serves as a notable imaging indicator of cerebral small vessel disease (CSVD) [2, 3], often presenting as distinct punctate or patchy abnormalities displaying high signal intensities in the white matter on T2-weighted imaging (T2WI) and fluid-attenuated inversion recovery (FLAIR) sequences [4, 5]. Depending on their locations, WMH can be classified as periventricular white matter hyperintensities (PWMH) and deep white matter hyperintensities (DWMH) [6–8].

WMH has been linked to a range of medical conditions and clinical results, including an elevated likelihood of experiencing a stroke and a less favorable prognosis after having a stroke [9, 10]. However, despite the established association between WMH and adverse stroke outcomes, existing prognostic models for AIS predominantly rely on clinical factors such as age, time of onset, stroke severity, stroke history, hypertension, and diabetes mellitus [11–13], or simplistic imaging metrics such as Fazekas scores [14, 15] or WMH volume [16, 17]. These approaches overlook the rich spatial and textural heterogeneity within WMH lesions, which may encode critical pathophysiological information about tissue vulnerability and recovery potential. Current studies analyzing WMH in AIS face three key limitations. First, prior radiomics-based AIS prognosis models primarily focus on acute infarct regions, neglecting the prognostic value of chronic WMH lesions readily detectable on routine FLAIR sequences. Second, conventional methods rely on manual visual ratings [1, 18] or basic morphological descriptors (e.g., volume, shape irregularity) [16, 17], primarily assess WMH in a limited, qualitative manner, failing to capture high-dimensional radiomic features that quantify subtle variations in lesion texture, edge sharpness, or wavelet patterns. Third, while machine learning algorithms have shown promise in medical imaging, their application to WMH radiomics for AIS prognosis remains underexplored, with most studies still employing logistic regression rather than advanced classifiers like SVM or autoencoders.

Over the past few years, radiomics has experienced a rapid growth in its advancement, being characterized as the process of high-throughput extraction and detailed analysis of numerous high-dimensional imaging features directly from medical images. By analyzing differences in image gray levels or pixel intensities, radiomics can describe tissue heterogeneity and quantify differences that are invisible to the human eye, which is important for the diagnosis and prognosis of the disease [19, 20]. Besides, most traditional studies use conventional LR models, while machine learning can offer a wider range of algorithms to comprehensively investigate the rich information buried in imaging [21]. In this respect, radiomics combined with machine learning can be used to conduct quantitative analysis on the features of WMH at various locations to predict AIS prognosis. By leveraging radiomics in combination with machine learning, we aim to overcome the current limitations in AIS prognosis prediction by utilizing a more sophisticated, data-driven approach that integrates both clinical and imaging features.

In this study, we identified various regions of interest (ROIs) of WMH in different locations on FLAIR sequence, extracted radiomics features, and constructed models using multiple machine learning methods. We first chose the most effective radiomics model to compute a Rad-score, which we then integrated with independent clinical predictors to develop a combined model. This model aims to investigate the utility of WMH radiomics features in predicting the 90-day functional outcomes of patients with AIS. Our primary research questions were: (1) Which location's WMH radiomics model has the best predictive efficacy for AIS prognosis? (2) Does combining the optimal WMH radiomics model with predictors improve the accuracy of prognostic prediction in AIS patients?

Materials and methods

Study population

This retrospective analysis encompassed 202 patients with AIS accompanied by WMH, who were admitted to the Neurology Department of Xuzhou Central Hospital between September 2023 and March 2024. The subjects were randomly assigned to training and validation

cohorts in a 7:3 ratio. Inclusion Criteria: (1) Patients diagnosed with AIS involving the anterior circulation; 2) receiving standard conservative treatment without a history of thrombolytic therapy (including endovascular treatment such as mechanical thrombectomy and arterial thrombolysis, and intravenous thrombolysis with alteplase or urokinase); 3) completion of cranial MRI scans, with DWI and ADC sequences confirming AIS and FLAIR sequence indicating WMH, with clear images meeting diagnostic requirements; 4) availability of complete clinical data. Exclusion Criteria: (1) AIS occurring in the posterior circulation; (2) large infarctions, cerebral hemorrhage, traumatic brain injury, brain tumors, arteriovenous malformations, or brain surgeries that may affect WMH lesion segmentation; (3) non-vascular origins of white matter lesions (such as demyelination, metabolic, toxic, or infectious causes); (4) cases of multiple sclerosis, Alzheimer's disease, and Parkinson's disease that have been confirmed through diagnosis; (5) Instances of severe head movement during MRI scanning that result in substandard image quality; (6) Failures in the segmentation of WMH; (7) Incomplete clinical data or discontinued follow-up assessments. Figure 1 depicts the meticulous patient selection process. This study, which has been granted approval by the Medical Ethics Committee of Xuzhou Central Hospital, dispenses with the need for informed consent from participants (approval number: XZXY-LK-20240709-0105).

Clinical data

Patient data was gathered from the hospital information system (HIS), encompassing fundamental demographic details, medical background, and laboratory findings during hospitalization period. This encompassed vital variables such as age, gender, hypertension, hyperlipidemia, diabetes mellitus (DM), coronary artery disease (CAD), prior stroke history, smoking and drinking habits, admission blood pressure, admission blood glucose levels, Hemoglobin A1c (HbA1c) concentrations, lipid profiles, homocysteine (HCY) amounts, and infarct volume size. For the collection of prognostic data, trained physicians conducted telephone interviews or outpatient follow-ups at 90 days post-stroke. These assessments employed the modified Rankin Scale (mRS) to evaluate functional outcomes. The prognosis was categorized as favorable with an mRS score ranging from 0 to 2, and unfavorable with a score of 3 to 6. Notably, the physicians were unaware of the patients' imaging data during the assessment process. The 90-day time point was chosen for prognostic evaluation in this study, as it is a widely accepted timeframe for assessing functional outcomes after AIS. Many clinical studies and guidelines utilize 90 days as the standard period for evaluating stroke recovery and functional outcomes [22–25]. This time point is considered optimal for assessing both short-term recovery and longer-term disability. Functional improvement was defined based on the change in the modified Rankin Scale (mRS) score. A clinically significant improvement was determined when a patient's mRS score decreased by at least one point, typically moving from a higher score (e.g., 3 or more) to

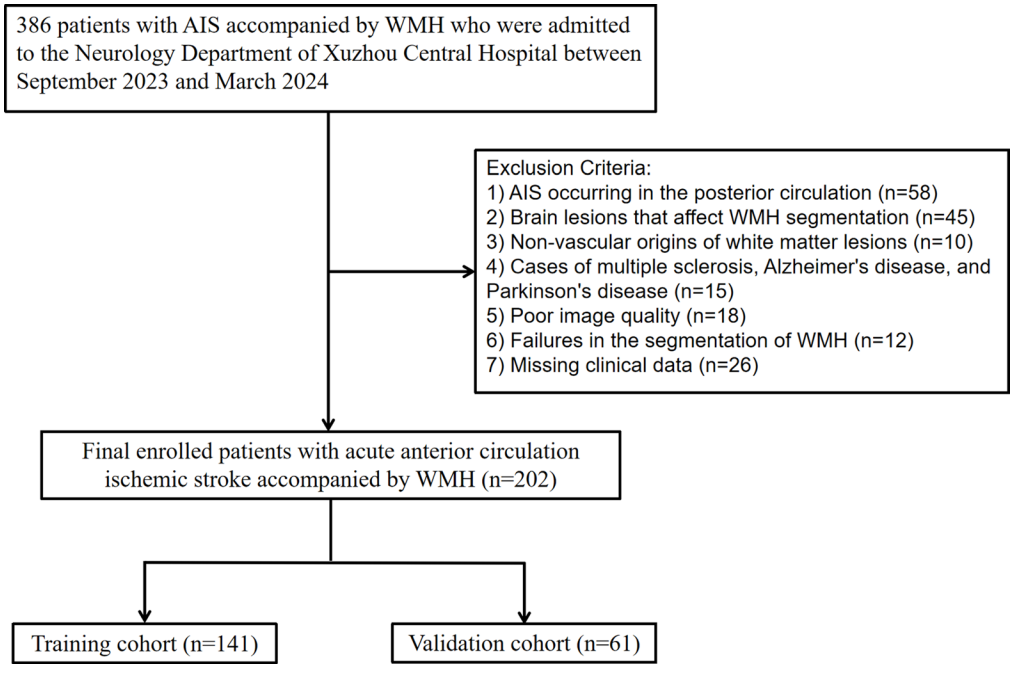

Fig. 1 Inclusion and exclusion flowchart of patients

a lower score (e.g., 2 or less). This definition is commonly used in AIS prognostic studies and reflects meaningful changes in patients' ability to perform daily activities and their quality of life.

MRI image acquisition

Upon admission, all enrolled patients underwent a comprehensive cranial MRI scan using high-end scanners. The MRI machines employed were either the GE Discovery 750w 3.0T or the Philips Ingenia 3.0T scanner for precise image acquisition. The scanning parameters were meticulously set to capture detailed images of the cranial structure and potential abnormalities. Specifically, the scanning parameters included: axial T1-weighted imaging (T1WI) with a repetition time (TR) ranging from 2000 to 2150 ms and an echo time (TE) of 15–28 ms; axial T2-weighted imaging (T2WI) with a TR of 2130–4300 ms and a TE of 80–130 ms; axial fluid-attenuated inversion recovery (FLAIR) sequence, which had a TR of 6000–9000 ms and a TE of 100 ms; and axial diffusion-weighted imaging (DWI) with a TR of 2773–5000 ms and a TE of 78–100 ms. The image slices were obtained with a thickness of 6.5 mm, an interslice gap of 1 mm and a field of view (FOV) spanning 230 mm across both horizontally and vertically. For the purpose of this study, the axial FLAIR images were primarily utilized for detailed analysis.

Radiomics analysis

Workflow

The radiomics analysis workflow comprises several key steps, WMH lesion segmentation, feature extraction and selection, as well as model construction and analysis (Fig. 2).

Image segmentation

FLAIR images in DICOM format were converted to NIFTY format using MATLAB (version 2023b; MathWorks). The converted images were imported into the SPM12 software package (SPM12, MATLAB version 2023b; MathWorks, Natick, MA). The utilization of the lesion segmentation toolbox (LST) (version 3.0.0), equipped with the lesion prediction algorithm (LPA) [26], was pivotal in the automatic segmentation of WMH lesions. This process was overseen by two experienced neurodiagnostic radiologists, possessing more than five years of expertise, who verified the segmentation outcomes with the ITK-SNAP software (version 4.0.2, accessible at http://www.itksnap.org/). Any discrepancies in segmentation were meticulously rectified by them to determine the final ROIs. The modifications undertaken included several steps:1) The initial step involved the elimination of non-brain tissue, along with the removal of the brainstem and cerebellar hyperintensities.2) Subsequently, adjustments were made to the white matter segmentation to exclude areas of apparent ischemia (AIS) that also appeared as hyperintensities on FLAIR images.

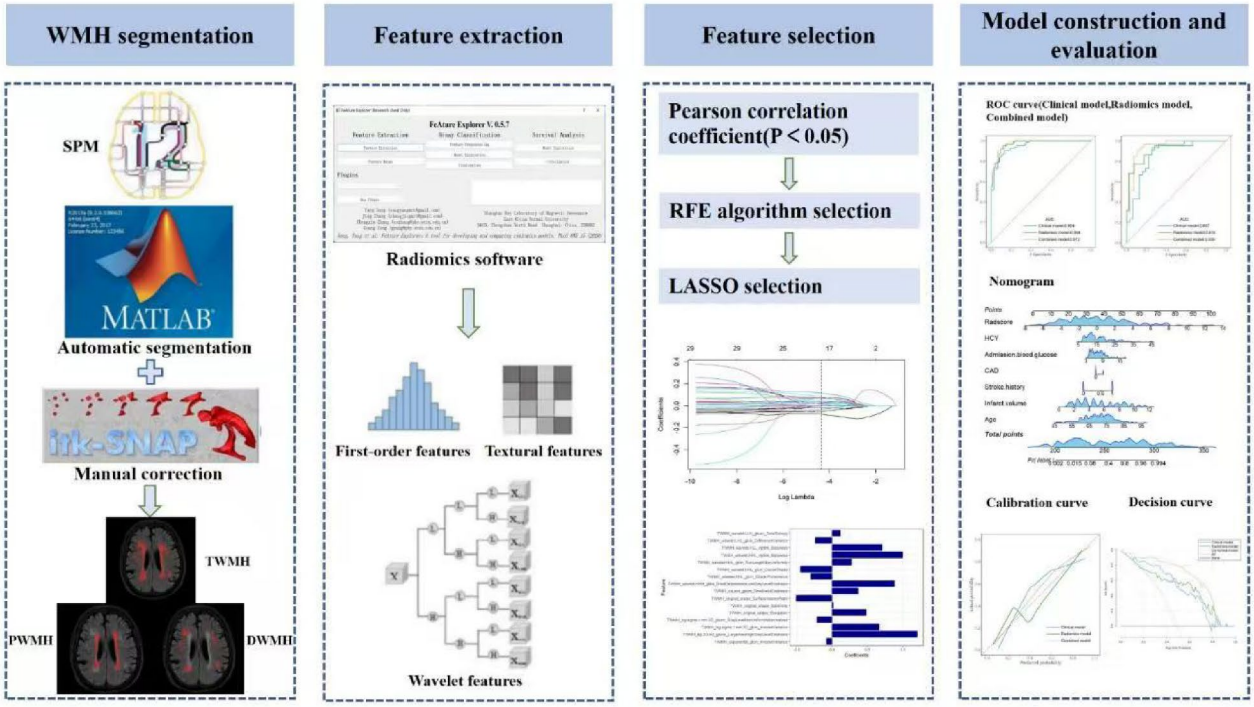

Fig. 2 Study flowchart of the radiomics analysis

After these corrections, the adjusted images were categorized as total white matter hyperintensities (TWMH). From this, PWMH and DWMH were meticulously outlined manually. Any disparities in interpretation between the two radiologists were resolved through extensive discussion and consensus building.

Feature extraction and selection

To ensure consistency in feature extraction across various MRI machines, all MRI images were resampled to uniform voxel sizes of 1 mm × 1 mm × 1 mm. Feature extraction was performed using the FAE software [27] (FeAture Explorer v. 0.5.7), which is developed in Python and utilizes the PyRadiomics library (version 3.0.1) as its core computational engine. We save the images and the ROIs in NFITY format and store the files for each case in a separate subfolder in a root folder. Next, set the root folder as the source folder and check the path exists. Then, configure the feature extraction parameters, including image type settings and feature type settings, including first-order features, shape descriptors, texture characteristics, wavelet transformation features, and features derived from the laplacian of gaussian filter transform. These algorithms for obtaining radiomics features were referenced from the Image Biomarker Standardization Initiative [28]. Each feature underwent Z-score normalization for standardization. To assess the reliability of image segmentation, a subset of 30 patients was randomly chosen. Two experienced neuroimaging diagnosticians, possessing over five years of expertise in the field, manually fine-tuned the automatically segmented lesion images to delineate ROIs. This procedure facilitated feature extraction while ensuring precision. The segmentation's consistency was assessed using the interclass correlation coefficient (ICC). Only radiomics features with an ICC value equal to or exceeding 0.8 were deemed reliable and subsequently utilized for further dimensionality reduction analysis.

The radiomics features from all ROIs were carefully screened in three systematic steps. Firstly, we analyzed the relationship between each feature and prognosis using the Pearson correlation coefficient (PCC). Thereby, features with statistical significance less than 0.05 were identified. Secondly, we employed the recursive feature elimination (RFE) algorithm to identify the top 30 relevant features, focusing on their importance for our analysis. Lastly, we applied the least absolute shrinkage and selection operator (LASSO) algorithm to determine the final set of features and their corresponding coefficients. This process provided valuable insights into the relative weightage assigned to each selected feature. Based on these chosen features and their coefficients, we create a feature importance plot, an extended visualization to better communicate our results.

Radiomics model construction

With the selected radiomics features, we developed different WMH location radiomics models by a variety of machine learning methods, including support vector machine (SVM), linear discriminant analysis (LDA), naive Bayes classifier (NB), logistic regression (LR), LASSO regression (LR-Lasso), and autoencoder (AE). In selecting machine learning classifiers, we strategically aligned model strengths with task requirements: 1)SVM: maximize classification margins using kernel methods, excelling in high-dimensional, small-sample medical imaging data; 2) LDA: optimizes inter-class variance for multiclass tasks with inherent dimensionality reduction; 3) NB: relying on feature independence assumptions, prioritizes computational efficiency but suits text-based applications better; 4) LR: provides probabilistic outputs and interpretability for clinical threshold determination; 5) LR-Lasso: employs L1 regularization for sparse feature selection, enhancing model generalizability; 6) AE: leverage nonlinear encoding to extract latent representations from multi-sequence MRI data. These classifiers have been widely used in constructing predictive models and have shown excellent performance. Meanwhile, regardless of the machine learning classifier used, we employed a stratified 5-fold cross-validation strategy to evaluate model performance and optimize hyperparameters. The validation set was used solely for final model performance evaluation and did not participate in any parameter optimization process. This strategy maximizes the use of data in cases of limited sample size while ensuring the stability of the evaluation results. The best combination of ROI and classifier was chosen to obtain the final radiomics model showing the best performance. Subsequently, the radiomics score (Rad-score) was determined by weighing the features and their corresponding coefficients, taking into account the context and classification techniques used.

Clinical and combined model construction

To identify independent clinical predictors and construct a clinical model, univariate and multivariate logistic regression analyses were employed, selecting clinical factors with a significance level of $P < 0.05$. These clinically significant predictors were then combined with the Rad-score from the most optimal radiomics model to develop an integrated clinical-radiomics model. The nomogram is generated based on the regression coefficients of the combined model. Each predictor is assigned a corresponding weighted score, and the total score is converted into the 90-day adverse prognosis probability for the patient through a calibration mapping function. The cutoff value for the Rad-score was determined through a receiver operating characteristic (ROC) curve analysis, aiming to identify the threshold that maximizes both

sensitivity and specificity [29]. This optimal cutoff value was selected by calculating the Youden Index, which balances the trade-off between false positive and false negative rates. The cutoff was initially determined using the training dataset and subsequently validated on the testing dataset.

Model evaluation

We generated receiver operating characteristic curves and calculated the area under the curve (AUC), sensitivity, specificity, and accuracy metrics for each model. In order to assess how well the models predict AIS prognosis, we conducted a comparative analysis of the AUC values. Additionally, we constructed calibration curves and performed decision curve analysis (DCA) to evaluate the predictive accuracy and clinical decision-making applicability of the models. The findings from these assessments provide valuable insights into both performance and practical usability of the models in real-world clinical settings.

Statistical analysis

A comprehensive statistical analysis was carried out utilizing the SPSS version 25.0 and R software (version 4.0.2). Initial assessments were conducted on the continuous variables through normality tests. Depending on the results, either the independent sample t-test or the Mann-Whitney U test was applied. The normally distributed data were expressed in terms of the mean ± standard deviation ($x \pm S$), while the non-normally distributed data were displayed using the median along with the upper and lower quartiles [M (P25, P75)]. For categorical variables, a χ^2 test was employed for analysis and expressed in terms of frequency (%). The significance level was determined by a two-tailed p-value of less than 0.05, which was considered statistically significant in terms of its implications.

Results

Comparison of clinical characteristics

The study initially included 386 patients with AIS accompanied by WMH. After applying the exclusion criteria, a total of 202 patients with acute anterior circulation ischemic stroke accompanied by WMH were ultimately enrolled, comprising 132 males and 70 females. The excluded cases comprised 58 patients with AIS occurring in the posterior circulation, 45 patients with brain lesions affecting WMH segmentation, 10 patients with non-vascular white matter lesions, 15 patients with multiple sclerosis, Alzheimer's disease, and Parkinson's disease, 18 patients with poor image quality, 12 patients with failed WMH segmentation, and 26 patients with missing clinical data. The patients were divided into two cohorts: the training cohort with 74 patients having a good prognosis and 67 with a poor prognosis, and the validation cohort with 31 patients showing a good prognosis and 30 indicating a poor prognosis. The baseline clinical characteristics or prognosis between these two cohorts did not exhibit any significant differences ($P > 0.05$). Table 1 presents the baseline clinical characteristics of the patients. Through extensive analysis, including univariate and multivariate logistic regression, independent clinical predictors of AIS prognosis were identified. These predictors included age, history of stroke, CAD, admission blood glucose level, homocysteine level, and infarct volume (Table 2). Using these five factors, a comprehensive clinical model was constructed to provide a better understanding of AIS prognosis.

Radiomics feature extraction and selection

The extraction of 1,688 features from three distinct ROIs, namely TWMH, PWMH, and DWMH, was accomplished through the FLAIR sequence. These features encompassed a range of categories, including first-order features, shape descriptors, texture characteristics, wavelet transformation features, and features derived from the laplacian of gaussian filter transform. Subsequent to rigorous filtering using PCC, RFE, and LASSO techniques, a subset of features was selectively chosen. Specifically, from TWMH, 16 features were selected (comprising of 3 shape descriptors, 3 texture characteristics, 8 wavelet transformation features, and 2 features from the Laplacian of Gaussian filter transform). In the case of PWMH, 21 features were chosen (including 6 texture characteristics, 11 wavelet transformation features, and 4 features from the Laplacian of Gaussian filter). Lastly, for DWMH, 22 features were handpicked (consisting of 9 texture characteristics, 12 wavelet transformation features, and 1 feature from the Laplacian of Gaussian filter).

Radiomics model construction and evaluation

Drawing upon the radiomics features meticulously extracted from TWMH, PWMH, and DWMH, we constructed predictive models utilizing six distinct classifiers: SVM, LDA, AE, LR, LR-Lasso, and NB. Table 3 shows a performance comparison of radiomics models constructed with different ROI and classifier combinations in the validation cohort, including sensitivity, specificity, accuracy, and AUC. The AUC values are visualized as a heatmap (Fig. 3) to better contrast the performance across models. Our results demonstrate that, irrespective of the classifier utilized, the AUC of the radiomics model based on TWMH consistently excelled those derived from PWMH and DWMH models in the validation cohort. Notably, the TWMH model employing the SVM classifier demonstrated superior performance (AUC of 0.968 in the training cohort and 0.916 in the validation cohort). The LASSO selection process and feature

Table 1 Comparison of prognosis and clinical baseline characteristics between the training and validation cohorts

Variables	Training cohort($n=141$)	Validation cohort($n=61$)	$t/\chi^2/Z$	*P*
Age (years)	70.05 ± 9.47	69.87 ± 7.30	0.133	0.894
Infarct volume (cm^3)	4.58(3.16,7.69)	4.38(2.53,6.94)	-1.097	0.273
Gender (%)			3.563	0.059
Female	43(30.5)	27(44.3)		
Male	98(69.5)	34(55.7)		
Hypertension (%)			0.356	0.551
No	38(27.0)	14(23.0)		
Yes	103(73.0)	47(77.0)		
Hyperlipidemia (%)			0.002	0.963
No	132(93.6)	57(93.4)		
Yes	9(6.4)	4(6.6)		
DM (%)			0.263	0.608
No	99(70.2)	45(73.8)		
Yes	42(29.8)	16(26.2)		
CAD (%)			1.418	0.234
No	97	47		
Yes	44	14		
Stroke history (%)			0.454	0.500
No	72(51.1)	28(45.9)		
Yes	69(48.9)	33(54.1)		
Smoking history (%)			0.097	0.755
No	101(71.6)	45(73.8)		
Yes	40(28.4)	16(26.2)		
Drinking history (%)			0.807	0.369
No	105(74.5)	49(80.3)		
Yes	36(25.5)	12(19.7)		
Systolic blood pressure (mmHg)	154.58 ± 22.60	152.25 ± 22.26	0.677	0.499
Diastolic blood pressure (mmHg)	88.51 ± 12.69	86.62 ± 13.01	0.964	0.336
Admission blood glucose (mmol/L)	7.15(5.26,8.79)	6.77(5.13,8.62)	-0.703	0.482
HbA1c (%)	6.10(5.75,7.30)	6.30(5.70,7.65)	-0.563	0.574
TC (mmol/L)	4.55(3.69,5.25)	4.25(3.69,4.80)	-1.214	0.225
TG (mmol/L)	1.28(0.87,1.76)	1.22(0.83,1.83)	-0.222	0.825
HDL (mmol/L)	1.17(0.97,1.34)	1.10(0.88,1.22)	-1.993	0.056
LDL (mmol/L)	2.77(2.02,3.34)	2.52(2.04,3.02)	-1.459	0.145
HCY (μmol/L)	13.79(11.28,18.94)	12.09(10.28,18.31)	-1.467	0.142
Prognosis (%)			0.047	0.828
Good (mRS 0–2)	74(52.5)	31(50.8)		
Poor (mRS 3–6)	67(47.5)	30(49.2)		

Abbreviations: t: t-test; Z: Mann-Whitney test; χ^2: Chi-square test; DM: Diabetes mellitus; CAD: coronary artery disease; HbA1c: Hemoglobin A1c; TC: total cholesterol; TG: triglyceride; HDL: high density lipoprotein; LDL: low density lipoprotein; HCY: homocysteine; mRS: the modified Rankin Scale

Table 2 Binary logistic regression analysis of clinical factors

Variables	β	Z	*P*	OR (95%CI)
Age	0.12	2.56	0.011	1.13(1.03 ~ 1.25)
Infarct Volume	0.26	2.08	0.037	1.29(1.02 ~ 1.65)
Admission blood glucose	0.32	2.39	0.017	1.37(1.06 ~ 1.78)
Stroke History	1.95	3.07	0.002	7.00(2.02 ~ 24.24)
CAD	1.72	2.36	0.018	5.58(1.34 ~ 23.28)
HCY	0.13	2.95	0.003	1.14(1.04 ~ 1.24)

Abbreviations: CI: confidence interval; CAD: coronary artery disease; HCY: homocysteine

importance plot are presented in Fig. 4. In the training cohort, this model exhibited sensitivity of 0.971, specificity of 0.973, and accuracy of 0.972. When validated, it achieved a sensitivity of 0.900, specificity of 0.813, and accuracy of 0.853. Consequently, this model was chosen as the definitive radiomics model. The Rad-score for each individual was computed based on the selected features and their corresponding coefficients, which were further integrated into the development of a comprehensive model.

Table 3 The performance of radiomics models combining different rois and classifiers in the validation cohort

ROI	Classifier	Sen	Spe	Acc	AUC (95%CI)
TWMH	SVM	0.897	0.813	0.853	0.916(0.849–0.983)
	LDA	0.931	0.781	0.853	0.909(0.836–0.983)
	AE	0.793	0.906	0.853	0.881(0.791–0.972)
	LR	0.897	0.875	0.885	0.906(0.832–0.980)
	LR-Lasso	0.897	0.875	0.885	0.911(0.839–0.982)
	NB	0.897	0.804	0.839	0.914(0.843–0.985)
PWMH	SVM	0.931	0.856	0.787	0.851(0.756–0.946)
	LDA	0.755	0.806	0.787	0.830(0.718–0.932)
	AE	0.686	0.816	0.754	0.778(0.661–0.895)
	LR	0.828	0.781	0.803	0.849(0.752–0.947)
	LR-Lasso	0.828	0.781	0.803	0.863(0.771–0.955)
	NB	0.724	0.906	0.630	0.878(0.791–0.964)
DWMH	SVM	0.690	0.813	0.754	0.763(0.640–0.886)
	LDA	0.759	0.875	0.820	0.818(0.705–0.931)
	AE	0.548	0.738	0.705	0.724(0.594–0.854)
	LR	0.690	0.813	0.754	0.782(0.665-0.900)
	LR-Lasso	0.690	0.813	0.754	0.788(0.673–0.903)
	NB	0.724	0.750	0.738	0.743(0.612–0.873)

Abbreviations: TWMH: Total White Matter Hyperintensities; PWMH: Periventricular White Matter Hyperintensities; DWMH: Deep White Matter Hyperintensities; SVM: support vector machine; LDA: linear discriminant analysis; AE: autoencoder; LR: logistic regression; LR-Lasso: LASSO regression; NB: naive Bayes; Sen: Sensitivity; Spe: Specificity; Acc: Accuracy; AUC: area under the curve; CI: confidence interval

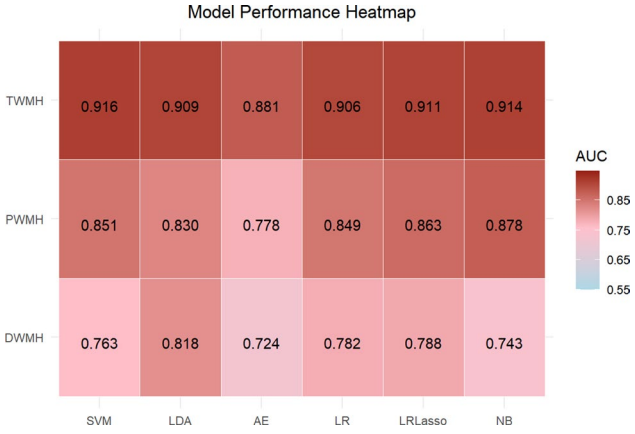

Fig. 3 AUC of machine learning predictive models based on radiomics features of TWMH, PWMH and DWMH

Construction and evaluation of the clinical-radiomics combined model

A logistic regression algorithm was utilized to integrate independent clinical predictors with the optimal radiomics Rad-score, resulting in the development of a combined model. The performance of this integrated model was assessed using ROC curves and AUC values, which are presented in Fig. 5 and Table 4 for both the training and validation cohorts. In the training cohort, the combined model demonstrated superior predictive accuracy with an AUC of 0.972. Similarly, in the validation cohort, the AUC of this model was found to be 0.939. These results indicate that the combined model outperformed both the clinical model and the radiomics model.

Construction and validation of the nomogram

To enhance the comprehension and visualization of the integrated model, we have devised a nomogram as an assessment instrument (Fig. 6). The nomogram clearly illustrates the relative significance of each variable in a conspicuous manner. In the forefront of the diagram, a scale is showcased, featuring a comprehensive list of predictive variables on the left side. Each variable is allocated a distinct score, and the segment lengths accurately depict their respective impact on forecasting AIS prognosis. By meticulously calculating the weighted scores of each variable for an individual patient, a comprehensive total score can be derived, which subsequently aids in determining the anticipated probability of AIS prognosis.

Model evaluation

The calibration curves for the clinical model, the optimal radiomics model, and the combined model were all plotted distinctly in Fig. 7. Through the Hosmer-Lemeshow test, it was determined that all models exhibited P-values exceeding 0.05, signifying their strong calibration capabilities. Notably, the combined model demonstrated the most remarkable agreement between predicted and actual outcomes in the prognosis of AIS, outperforming the other two models in calibration accuracy. Further analysis through DCA, as presented in Fig. 8, revealed that the combined model consistently displayed a higher AUC in both the training and validation cohorts compared to the clinical and radiomics models. This indicates that across various high-risk thresholds, the combined model offers a greater clinical net benefit compared to the individual clinical and radiomics models, as well as the strategies of "intervening on all" or "intervening on none."

Discussion

In this research, we derived radiomics features from various WMH locations using FLAIR images. The most effective radiomics model was subsequently integrated with baseline patient data to assess the predictive accuracy of combined model in evaluating the prognosis of AIS patients. Initially, multivariate logistic regression analysis disclosed that age, CAD, prior stroke history, admission blood glucose levels, homocysteine concentrations, and infarct volume are independent clinical predictors with significant prognostic value. Subsequently, an examination of numerous radiomics prediction models revealed that the model encompassing both PWMH and DWMH, termed the TWMH model, demonstrated superior performance. Utilizing the SVM classifier, the TWMH

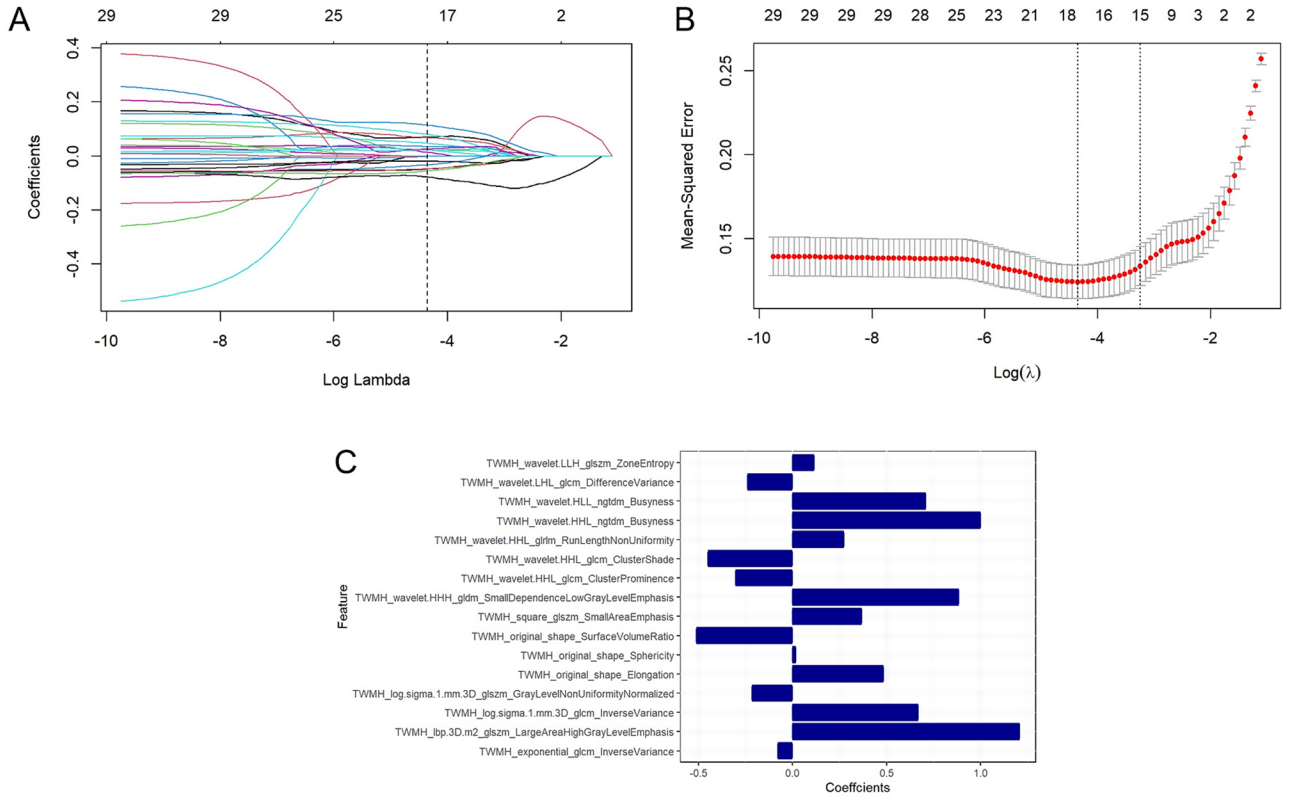

Fig. 4 Overview of the LASSO selection process for TWMH radiomics **(A, B)** and retained feature importance plot **(C)**

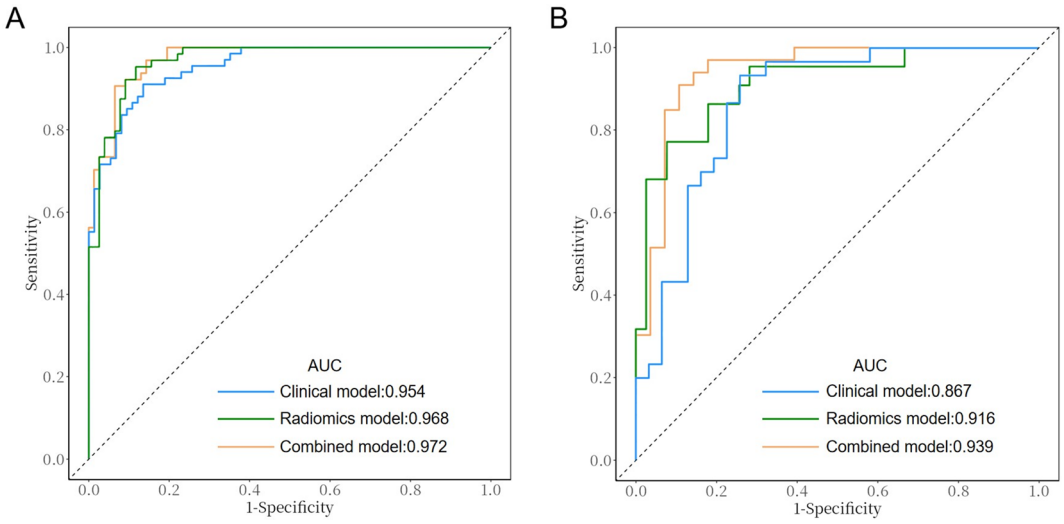

Fig. 5 ROC curves of the clinical model, radiomics model, and combined model in the training **(A)** and validation **(B)** cohort. ROC receiver operating characteristic

Table 4 Performance of the clinical model, radiomics model, and combined model

Model	Training cohort				Validation cohort			
	Sen	Spe	Acc	AUC (95%CI)	Sen	Spe	Acc	AUC (95%CI)
Clinical Model	0.865	0.910	0.887	0.954(0.924–0.983)	0.774	0.800	0.787	0.867(0.773–0.960)
Radiomics Model	0.971	0.973	0.972	0.968(0.935-1.000)	0.897	0.813	0.853	0.916(0.849–0.983)
Combined Model	0.935	0.906	0.922	0.972(0.951–0.993)	0.893	0.848	0.869	0.939(0.878–0.999)

Abbreviations: Sen: Sensitivity; Spe: Specificity; Acc: Accuracy; AUC: area under the curve; CI: confidence interval

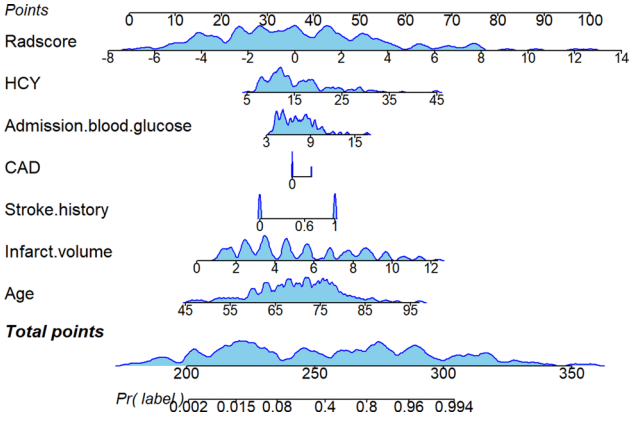

Fig. 6 A nomogram based on clinical-radiomics combined model for predicting AIS outcomes

radiomics model, grounded in FLAIR sequences, exhibited unparalleled predictive accuracy. To enhance the model's predictive capability, a nomogram was developed by amalgamating various clinical factors. Furthermore, the enhanced predictive performance of the combined model was further underscored through DCA, which also facilitated a comparative assessment of the clinical utility of each model component.

In recent times, radiomics has experienced rapid growth as a non-invasive analytical technique that enables the automated extraction of high-dimensional characteristics. Radiomics characteristics are highly effective in describing the distribution of grayscale and voxel relationships within images, thereby quantifying internal heterogeneity in lesions that cannot be visually perceived. This facilitates the comprehensive quantification of medical images, enhancing the role of imaging data in disease diagnosis and prognostic prediction [30–37]. Currently, numerous studies have developed prognostic prediction models for AIS by extracting radiomic features from lesions identified on multimodal MRI sequences [38–40]. Notably, Yu et al. constructed a radiomics model incorporating features simultaneously derived from DWI, ADC, FLAIR, SWI, and T1-weighted

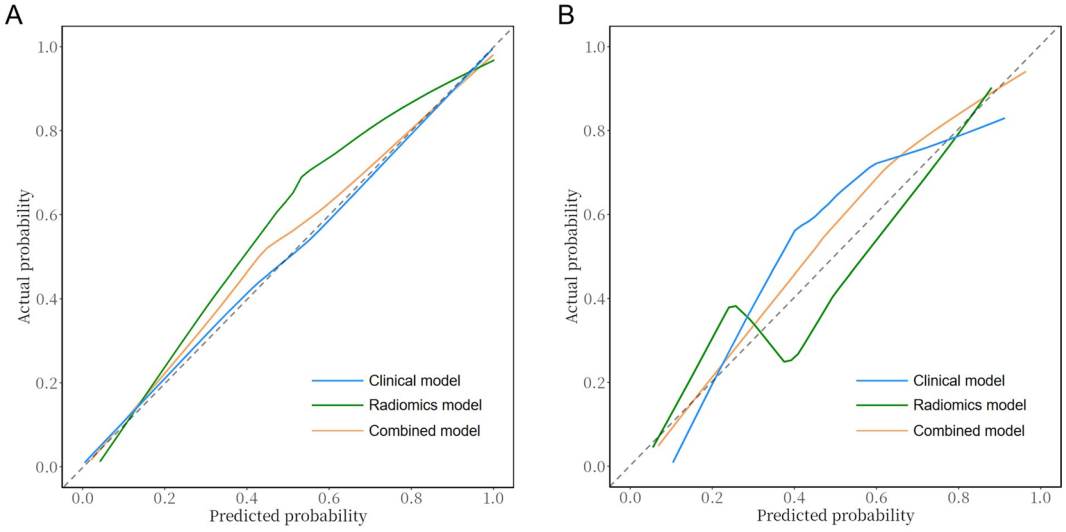

Fig. 7 Calibration curves of the clinical model, radiomics model, and combined model in the training **(A)** and validation **(B)** cohort

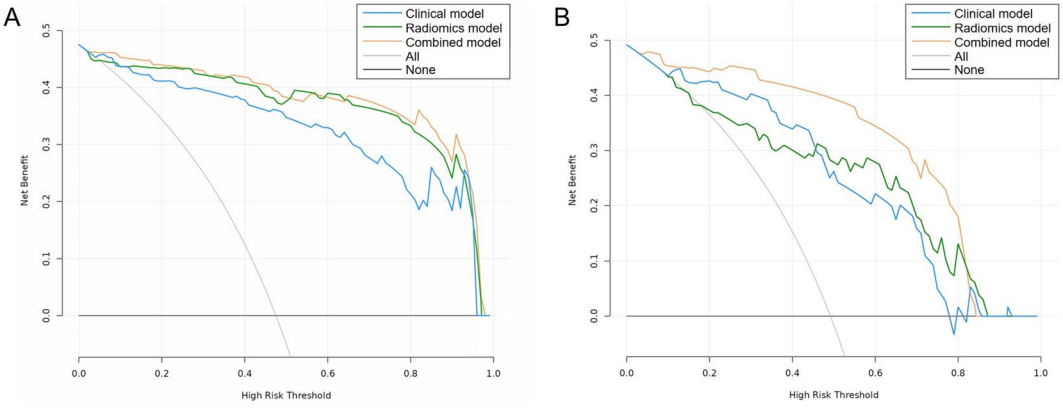

Fig. 8 Decision curve analysis of the clinical model, radiomics model, and combined model in the training **(A)** and validation **(B)** cohort

sequences, which achieved an AUC exceeding 0.90 in predicting AIS prognosis [40]. However, these studies primarily concentrate on stroke lesion areas with limited exploration into the association between WMH, commonly observed in imaging scans, and AIS prognosis. A few studies have reported that AIS patients with higher WMH burden face an elevated risk of unfavorable outcomes. For example, Christoph J. Griessenauer et al. demonstrated that increased WMH volume within a specific range is significantly correlated with 90-day functional outcomes in AIS patients [16], while Rashid Ghaznawi et al. found that larger and more irregularly shaped WMH is associated with a higher risk of vascular death in AIS [17]. However, these studies' analyses of WMH are limited to simple visual ratings or morphological indicators, which fail to capture the comprehensive information contained within WMH. To address this gap, our study innovatively extracts radiomics features from WMH in different locations based on the FLAIR sequence and utilized machine learning algorithms to assess the predictive capability of WMH radiomics features for AIS prognosis. Our results indicate that the TWMH radiomics model exhibited the best predictive performance, outperforming both PWMH and DWMH models. The SVM classifier achieved the best predictive accuracy, with an AUC of 0.968 in the training cohort and 0.916 in the validation cohort. We hypothesize that the superior performance of the TWMH model may be attributed to its coverage of the entire WMH lesion, allowing the extracted features to better represent subtle differences between pathological and normal tissues. These findings suggest that a more comprehensive inclusion of lesion tissues in clinical research can provide broader imaging information. Furthermore, the PWMH models, constructed using six different machine learning methods, consistently outperformed the DWMH models in predictive efficacy. This aligns with previous studies [1, 17], which indicated that PWMH is more sensitive than DWMH in predicting AIS prognosis. This may be attributed to their distinct pathophysiological mechanisms: (1) PWMH is associated with a more pronounced hypoperfusion mechanism. The periventricular white matter is located in a watershed area and primarily supplied by terminal arteries, making its blood supply more unstable, thus rendering it more susceptible to hemodynamic disturbances and ischemic manifestations [2, 41]; (2) The occurrence of DWMH is primarily related to the disruption of the BBB and increased interstitial fluid [42], with DWMH showing more axonal damage, vacuolation, and demyelination [43].

We extracted and selected 16 independent radiomics features from the TWMH lesions, including 3 shape features, 3 texture features, 8 wavelet transform features, and 2 Laplacian of Gaussian filter features. These features are critical for predicting AIS prognosis, as they provide a comprehensive depiction of the heterogeneity of WMH in AIS patients. They also offer a certain degree of explanation regarding the potential impact of WMH pathology on AIS prognosis. The elevated components within these feature analyses were associated with poorer AIS outcomes, further quantifying specific imaging biomarkers related to the prognosis of AIS in connection with WMH.

Our clinical model suggests that poor prognosis in AIS can be predicted by factors such as advanced age, coronary heart disease, a history of stroke, high blood sugar levels, elevated homocysteine levels, and a large infarct volume. This aligns with the results of several studies that have shown a direct correlation between hyperglycemia and an elevated likelihood of unfavorable outcomes in AIS [44–46]. This may be due to hyperglycemia exacerbating mitochondrial damage in the ischemic penumbra, resulting in acidosis within the infarct area, which worsens ischemic brain injury. Additionally, hyperglycemia causes BBB disruption, worsening cerebral edema, which further aggravates brain injury and hinders symptom recovery in AIS patients [45]. Therefore, actively controlling blood glucose in AIS patients plays a crucial role in improving neurological outcomes. Since CAD and AIS share certain similar mechanisms, CAD patients are at higher risk of cardiovascular complications after an acute AIS episode, which partially contributes to poorer AIS prognosis [47]. Zhong et al.'s study [48] discovered a notable association between homocysteine levels and prognosis in patients with AIS. This could be due to heightened oxidative stress caused by increased homocysteine levels leading to inflammation-induced damage to endothelial cells as well as stimulation of vascular smooth muscle cell proliferation, thereby worsening atherosclerosis. Consequently, this elevates the likelihood of early neurological decline and mortality among individuals with AIS. Extensive research has indicated that relying solely on either clinical or radiomics models tends to yield inconsistent outcomes. Henceforth, we integrated both clinical factors and radiomics features into an amalgamated model for enhanced accuracy in prediction. Our conclusive findings demonstrate that when compared separately against individual clinical or radiomics models, this combined approach exhibits optimal predictive performance while also showcasing superior calibration ability alongside practicality for real-world application in clinics.in the training cohort, it achieved a sensitivity of 0.935, specificity of 0.906, and an accuracy rate of 0.922. When applied to the validation cohort, the model displayed sensitivity of 0.893, specificity of 0.848, and an accuracy level of 0.869. While there may be slight fluctuations in these metrics, the model consistently exhibits excellent performance across various measurements and can be proved to be valuable and constructive in clinical practice. First,

this model provides clinicians with a risk assessment tool based on multidimensional data, helping to improve the accuracy of AIS prognosis evaluation. By comprehensively analyzing radiomics features and clinical data, doctors can gain a full understanding of a patient's risk status, enabling more personalized and precise treatment decisions. This model not only enhances decision-making efficiency and shortens the time required for AIS prognosis evaluation, but it also has the potential to improve cost-effectiveness. The automatic extraction of radiomics features combined with clinical data analysis reduces reliance on manual data interpretation, thereby lowering diagnostic and consultation costs. Additionally, the nomogram, as a visualization tool for the combined model, further simplifies the decision-making process for clinicians. By integrating multiple clinical variables and Rad-scores into an intuitive diagram, the nomogram provides doctors with a simple and efficient way to assess individualized patient risk. In clinical practice, physicians can use the nomogram to quickly calculate a patient's total risk score based on their specific data. Each variable on the nomogram has a corresponding score, and doctors can sum the scores of different factors based on the patient's condition to arrive at a risk score, which then guides the treatment plan. The nomogram provides clinicians with a quantifiable assessment tool, reducing bias from subjective judgment. Its applicability across diverse hospital settings, particularly in resource-limited regions, underscores its popularity and practicality.

There are certain limitations within this study. First, as a single-center retrospective investigation with a small sample size and the absence of an external validation cohort to evaluate the model's predictive performance, the clinical and demographic characteristics of patients from a single institution may differ from those in other hospitals or regions. Consequently, the study population may not fully represent broader populations, potentially compromising the generalizability and external validity of the model. Second, variability in post-discharge rehabilitation care—influenced by patients' socioeconomic status and access to healthcare resources—may introduce heterogeneity in mRS scores. Furthermore, this study employed a semi-automated segmentation technique that involved manual adjustments for regions of interest. While this method demonstrated a certain level of accuracy, it did introduce subjectivity during the exclusion of AIS lesions while delineating WMH lesions. To address these limitations, we will further conduct large-scale, prospective, multicenter studies incorporating broader cohorts and external validation cohorts to strengthen the robustness of the predictive model, while exploring deep learning-based lesion segmentation methods to enhance the precision of feature analysis.

Conclusion

In conclusion, this study conducted a comprehensive radiomics feature analysis of WMH across distinct brain regions, identifying the most robust imaging biomarkers through advanced machine learning techniques. Furthermore, we developed and validated a potent nomogram integrating clinical risk factors with TWMH radiomics features to predict 90-day functional outcomes in AIS patients following conservative management. The combined model demonstrated superior predictive performance, achieving AUCs of 0.972 and 0.939 in the training and validation cohorts, respectively. Future research should prioritize prospective multicenter validation with expanded sample sizes and incorporation of automated segmentation algorithms to enhance the model's robustness, applicability, and generalizability.

Abbreviations

MRI	Magnetic resonance imaging
WMH	White matter hyperintensities
AIS	Acute ischemic stroke
FLAIR	Fluid-attenuated inversion recovery
TWMH	Total white matter hyperintensities
PWMH	Periventricular white matter hyperintensities
DWMH	Deep white matter hyperintensities
ROI	Region of interest
CSVD	Cerebral small vessel disease
T2WI	T2-weighted imaging
BBB	Blood-brain barrier
ASL	Arterial spin labeling
HIS	Hospital information system
DM	Diabetes mellitus
CAD	Coronary artery disease
HbA1c	Hemoglobin A1c
HCY	Homocysteine
mRS	modified rankin scale
T1WI	T1-weighted imaging
TR	Repetition time
TE	Echo time
DWI	Diffusion-weighted imaging
FOV	Field of view
LST	Lesion segmentation toolbox
LPA	Lesion prediction algorithm
ICC	Interclass correlation coefficient
PCC	Pearson correlation coefficient
RFE	Recursive feature elimination
LASSO	The least absolute shrinkage and selection operator
SVM	Support vector machine
LDA	Linear discriminant analysis
NB	Naive baye
LR	Logistic regression
LR-Lasso	LASSO regression
AE	Autoencoder
ROC	Receiver operating characteristic
AUC	Area under the curve
DCA	Decision curve analysis
ASPECTS	Alberta stroke program early CT score
DCE MRI	Dynamic contrast-enhanced magnetic resonance imaging

Supplementary Information

The online version contains supplementary material available at https://doi.org/10.1186/s12880-025-01632-1.

Supplementary Material 1

Acknowledgements
Not applicable.

Author contributions
Xia was responsible for conceptualization; Xia, Li and Zhai were responsible for data analysis; Zhai, Liu and Shi were responsible for supervision; Xia and Li wrote the manuscript; Xia, Liu and Shi were responsible for the experimental design; Shi reviewed and edited the manuscript; Shi contributed to project management and funding acquisition. All authors have read and agreed to publish the manuscript.

Funding
This research was supported by grants from Wu Jieping Medical Foundation Clinical Research Special Fund Project (320.6750.2023-11-24).

Data availability
All data generated or analyzed during this study are included in this published article.

Declarations

Ethics approval and consent to participate
This study was conducted in accordance with the Declaration of Helsinki (as revised in 2013) and was approved by the Medical Ethics Committee of Xuzhou Central Hospital (ethical batch number: XZXY-LK-20240709-0105). Because of the retrospective nature of the study, the requirement for informed consent was waived with the approval of Medical Ethics Committee of Xuzhou Central Hospital. All methods were carried out in accordance with relevant guidelines and regulations.

Consent for publication
Not applicable.

Competing interests
The authors declare no competing interests.

Author details
[1]The Affiliated Xuzhou Clinical College of Xuzhou Medical University, Xuzhou 221009, China
[2]Department of Radiology, Affiliated Hospital of Nantong University, Medical School of Nantong University, Nantong 226001, China
[3]Department of Radiology, Xuzhou Central Hospital, No. 199, Jiefang South Road, Quanshan District, Xuzhou City, Jiangsu Province 221009, PR China
[4]Department of Radiology, Nanyang First People's Hospital, Nanyang 473000, China

Received: 31 October 2024 / Accepted: 11 March 2025
Published online: 19 March 2025

References

1. Wang X, Lyu J, Meng Z, Wu X, Chen W, Wang G, Niu Q, Li X, Bian Y, Han D, et al. Small vessel disease burden predicts functional outcomes in patients with acute ischemic stroke using machine learning. CNS Neurosci Ther. 2023;29(4):1024–33.
2. Wardlaw JM, Smith EE, Biessels GJ, Cordonnier C, Fazekas F, Frayne R, Lindley RI, O'Brien JT, Barkhof F, Benavente OR, et al. Neuroimaging standards for research into small vessel disease and its contribution to ageing and neurodegeneration. Lancet Neurol. 2013;12(8):822–38.
3. Ostergaard L, Engedal TS, Moreton F, Hansen MB, Wardlaw JM, Dalkara T, Markus HS, Muir KW. Cerebral small vessel disease: capillary pathways to stroke and cognitive decline. J Cereb Blood Flow Metabolism: Official J Int Soc Cereb Blood Flow Metabolism. 2016;36(2):302–25.
4. Zhou R, Cai Q, Liu C, Hui J, Kang M, Gou Y, Liu Y, Shi P, Wang B, Zhang F. Association between white matter hyperintensity and anxiety/depression. Cereb Cortex. 2024;34(4).
5. Prins ND, Scheltens P. White matter hyperintensities, cognitive impairment and dementia: an update. Nat Rev Neurol. 2015;11(3):157–65.
6. DeCarli C, Fletcher E, Ramey V, Harvey D, Jagust WJ. Anatomical mapping of white matter hyperintensities (WMH): exploring the relationships between periventricular WMH, deep WMH, and total WMH burden. Stroke. 2005;36(1):50–5.
7. Zhang Y, Chang P, Liu N, Jiang Y, Chu Y, Du W, Lin L, Gao B, Li Y, Qu M, et al. Correlation between lenticulostriate arteries and white matter microstructure changes in patients with cerebral small vessel disease. Front Neurosci. 2023;17:1202538.
8. Yang YH, Li SS, Wang YC, Yu LL, Zhu HH, Wu JH, Yu WK, An L, Yuan WX, Ji Y, et al. Correlation between neutrophil gelatinase phase Lipocalin and cerebral small vessel disease. Front Neurol. 2023;14:1177479.
9. Rost NS, Cougo P, Lorenzano S, Li H, Cloonan L, Bouts MJ, Lauer A, Etherton MR, Karadeli HH, Musolino PL, et al. Diffuse microvascular dysfunction and loss of white matter integrity predict poor outcomes in patients with acute ischemic stroke. J Cereb Blood Flow Metabolism: Official J Int Soc Cereb Blood Flow Metabolism. 2018;38(1):75–86.
10. Hong S, Giese AK, Schirmer MD, Bonkhoff AK, Bretzner M, Rist P, Dalca AV, Regenhardt RW, Etherton MR, Donahue KL, et al. Excessive white matter hyperintensity increases susceptibility to poor functional outcomes after acute ischemic stroke. Front Neurol. 2021;12:700616.
11. Xing Y, Jin Y, Liu Y. Construction and comparison of short-term prognosis prediction model based on machine learning in acute ischemic stroke. Heliyon. 2024;10(1):e24232.
12. Ding GY, Xu JH, He JH, Nie ZY. Clinical scoring model based on age, NIHSS, and stroke-history predicts outcome 3 months after acute ischemic stroke. Front Neurol. 2022;13:935150.
13. Ling X, Shen B, Li K, Si L, Yang X. Development of a prediction model for 1-year poor prognosis in patients with acute ischemic stroke. J Investig Med. 2019;67(6):957–63.
14. Oussoren FK, Poulsen LNF, Kardux JJ, Schermer TR, Bruintjes TD, van Leeuwen RB. Cerebral small vessel disease in elderly patients with vestibular neuritis. Front Neurol. 2022;13:818533.
15. McBride CA, Russom Z, Achenbach E, Bernstein IM, Dumas JA. Cardiovascular profiles associated with white matter hyperintensities in healthy young women. Front Physiol. 2022;13:979899.
16. Griessenauer CJ, McPherson D, Berger A, Cuiper P, Sofoluke N, Adams MD, Kunaprayoon S, Zand R, Li J, Abedi V, et al. Effects of white matter hyperintensities on 90-Day functional outcome after large vessel and Non-Large vessel stroke. Cerebrovasc Dis. 2020;49(4):419–26.
17. Ghaznawi R, Geerlings MI, Jaarsma-Coes M, Hendrikse J, de Bresser J, Group UC-SS. Association of white matter hyperintensity markers on MRI and Long-term risk of mortality and ischemic stroke: the SMART-MR study. Neurology. 2021;96(17):e2172–83.
18. Nan Z, Lei Z, Yao W, Shuwei B, Jieli G, Ling Y, Wenwei C, Lei Z, Yan Z, Yangtai G. Modified cerebral small vessel disease score is associated with vascular cognitive impairment after lacunar stroke. Aging. 2021;12(7).
19. Lambin P, Leijenaar RTH, Deist TM, Peerlings J, de Jong EEC, van Timmeren J, Sanduleanu S, Larue R, Even AJG, Jochems A, et al. Radiomics: the Bridge between medical imaging and personalized medicine. Nat Rev Clin Oncol. 2017;14(12):749–62.
20. Zhang K, Zhou X, Xi Q, Wang X, Yang B, Meng J, Liu M, Dong N, Wu X, Song T et al. Outcome prediction of spontaneous supratentorial intracerebral hemorrhage after surgical treatment based on Non-Contrast computed tomography: A multicenter study. J Clin Med. 2023:12(4).
21. Fei W. Machine learning for predicting rare clinical Outcomes-Finding needles in a haystack. JAMA Netw Open. 2021;4(5):e2110738–2110738.
22. Kaveeta C, Alhabli I, Bala F, Horn M, Benali F, Coutts SB, Zafar A, Bereznyakova O, Khaw A, Khosravani H, et al. The treatment effect across ASPECTS in acute ischemic stroke: analysis from the act trial. Int J Stroke. 2024;20(1):64–74.
23. Liu L, Nguyen TN, Chen H-S. Endovascular treatment for acute ischemic stroke in China: a study protocol for a prospective, National, multi-center, registry study. Front Neurol. 2023;14.
24. Peng Z, Song J, Li L, Guo C, Yang J, Kong W, Huang J, Hu J, Liu S, Tian Y, et al. Association between stress hyperglycemia and outcomes in patients with acute ischemic stroke due to large vessel occlusion. CNS Neurosci Ther. 2023;29(8):2162–70.
25. Pei C, He C, Li H, Li X, Huang W, Liu J, Yin J. Clinical and imaging markers for the prognosis of acute ischemic stroke. Front Neurol. 2024;15.
26. Gaubert M, Dell'Orco A, Lange C, Garnier-Crussard A, Zimmermann I, Dyrba M, Duering M, Ziegler G, Peters O, Preis L, et al. Performance evaluation of automated white matter hyperintensity segmentation algorithms in a

multicenter cohort on cognitive impairment and dementia. Front Psychiatry. 2023:13.
27. Song Y, Zhang J, Zhang YD, Hou Y, Yan X, Wang Y, Zhou M, Yao YF, Yang G. FeAture explorer (FAE): A tool for developing and comparing radiomics models. PLoS ONE. 2020;15(8):e0237587.
28. Fornacon-Wood I, Mistry H, Ackermann CJ, Blackhall F, McPartlin A, Faivre-Finn C, Price GJ, O'Connor JPB. Reliability and prognostic value of radiomic features are highly dependent on choice of feature extraction platform. Eur Radiol. 2020;30(11):6241–50.
29. Tsai YT, Tsai MH, Kudva A, Vito A, Lai CH, Liao CT, Kang CJ, Tsai YH, Hsu CM, Huang EI, et al. The prognostic value of preoperative total cholesterol in surgically treated oral cavity cancer. Biomedicines 2024:12(12).
30. E MM, Andrzej M, Georg L, Ida H, Piotr S, Peter G, Gary C. Introduction to radiomics. J Nuclear Medicine: Official Publication Soc Nuclear Med. 2020;61(4):488–95.
31. van Timmeren JE, Cester D, Tanadini-Lang S, Alkadhi H, Baessler B. Radiomics in medical imaging-how-to guide and critical reflection. Insights Imaging. 2020;11(1):91.
32. Sun QC, Chen YS, Liang CF, Zhao YS, Lv XF, Zou Y, Yan K, Zheng HR, Liang D, Li ZC. Biologic pathways underlying prognostic radiomics phenotypes from paired MRI and RNA sequencing in glioblastoma. Radiology. 2021;301(3):654–63.
33. Yan J, Zhao Y, Chen Y, Wang W, Duan W, Wang L, Zhang S, Ding T, Liu L, Sun Q, et al. Deep learning features from diffusion tensor imaging improve glioma stratification and identify risk groups with distinct molecular pathway activities. EBioMedicine. 2021;72:103583.
34. Zhang S, Song M, Zhao Y, Xu S, Sun Q, Zhai G, Liang D, Wu G, Li ZC. Radiomics nomogram for preoperative prediction of progression-free survival using diffusion-weighted imaging in patients with muscle-invasive bladder cancer. Eur J Radiol. 2020;131:109219.
35. Wu WX, Yan J, Zhao YS, Sun QC, Zhang HL, Cheng JL, Liang D, Chen YS, Zhang ZY, Li ZC. Multi-task learning for concurrent survival prediction and semi-supervised segmentation of gliomas in brain MRI. Displays 2023;78.
36. You HX, Zhao YS, Sun QC, Wu WX, Lv XF, Chen YS, Zhang HL, Li ZC. Deep learning MRI signature to predict survival and treatment benefit from Temozolomide in IDH-wildtype glioblastoma. Displays 2023:77.
37. You HX, Zhang JK, Zhao YS, Mo T, Fang DA, Lv XF, Li ZC, Wang HF, Liang D, Zeng HW, et al. Riskformer: survival prediction from MR imaging in patients with IDH-wildtype glioblastoma. Displays. 2023:79.
38. Zhou Y, Wu D, Yan S, Xie Y, Zhang S, Lv W, Qin Y, Liu Y, Liu C, Lu J, et al. Feasibility of a Clinical-Radiomics model to predict the outcomes of acute ischemic stroke. Korean J Radiol. 2022;23(8):811–20.
39. Quan G, Ban R, Ren JL, Liu Y, Wang W, Dai S, Yuan T. FLAIR and ADC Image-Based radiomics features as predictive biomarkers of unfavorable outcome in patients with acute ischemic stroke. Front Neurosci. 2021;15:730879.
40. Yu H, Wang Z, Sun Y, Bo W, Duan K, Song C, Hu Y, Zhou J, Mu Z, Wu N. Prognosis of ischemic stroke predicted by machine learning based on multi-modal MRI radiomics. Front Psychiatry. 2022;13:1105496.
41. Dolui S, Tisdall D, Vidorreta M, Jacobs DR Jr., Nasrallah IM, Bryan RN, Wolk DA, Detre JA. Characterizing a perfusion-based periventricular small vessel region of interest. Neuroimage Clin. 2019;23:101897.
42. Iordanishvili E, Schall M, Loucao R, Zimmermann M, Kotetishvili K, Shah NJ, Oros-Peusquens AM. Quantitative MRI of cerebral white matter hyperintensities: A new approach towards Understanding the underlying pathology. NeuroImage. 2019;202:116077.
43. Jiang J, Gao Y, Zhang R, Wang L, Zhao X, Dai Q, Zhang W, Xu X, Chen X. Differential effects of serum Lipoprotein-Associated phospholipase A2 on periventricular and deep subcortical white matter hyperintensity in brain. Front Neurol. 2021;12:605372.
44. Guo K, Zhu B, Li R, Xi J, Wang Q, Chen K, Shao Y, Liu J, Cao W, Liu Z, et al. Machine learning-based nomogram: integrating MRI radiomics and clinical indicators for prognostic assessment in acute ischemic stroke. Front Neurol. 2024:15.
45. Jin L, Wenbo L, Jianping S, Xinyi G, Qiang M, Weijun T. Analysis of the risk factors for the short-term prognosis of acute ischemic stroke. Int J Clin Exp Med. 2015;8(11):21915–24.
46. E CM, E PJ IPL. Acute ischemic stroke and hyperglycemia. Crit Care Nurs Q. 2014;37(2):182–7.
47. Yousufuddin M, Bartley AC, Alsawas M, Sheely HL, Shultz J, Takahashi PY, Young NP, Murad MH. Impact of multiple chronic conditions in patients hospitalized with stroke and transient ischemic attack. J Stroke Cerebrovasc Dis. 2017;26(6):1239–48.
48. Zhong C, Xu T, Xu T, Peng Y, Wang A, Wang J, Peng H, Li Q, Geng D, Zhang D, et al. Plasma homocysteine and prognosis of acute ischemic stroke: a Gender-Specific analysis from CATIS randomized clinical trial. Mol Neurobiol. 2017;54(3):2022–30.

Publisher's note